Reaction mechanisms of atomic layer deposition of TaNx from Ta(NMe2)5 precursor and H2-based plasmas

Reaction mechanisms of atomic layer deposition of TaN_x from $Ta(NMe_2)_5$ precursor and H_2-based plasmas

H. C. M. Knoops
Materials innovation institute M2i, P.O. Box 5008, 2600 GA Delft, The Netherlands and Eindhoven University of Technology, P.O. Box 513, 5600 MB Eindhoven, The Netherlands

E. Langereis, M. C. M. van de Sanden, and W. M. M. Kessels[a)]
Eindhoven University of Technology, P.O. Box 513, 5600 MB Eindhoven, The Netherlands

(Received 4 March 2011; accepted 22 June 2011; published 26 August 2011)

The reaction mechanisms of plasma-assisted atomic layer deposition (ALD) of TaN_x using $Ta(NMe_2)_5$ were studied using quadrupole mass spectrometry (QMS). The fact that molecule dissociation and formation in the plasma have to be considered for such ALD processes was illustrated by the observation of 4% NH_3 in a H_2-N_2 (1:1) plasma. Using QMS measurements the reaction products during growth of conductive TaN_x using a H_2 plasma were determined. During the $Ta(NMe_2)_5$ exposure the reaction product $HNMe_2$ was detected. The amount of adsorbed $Ta(NMe_2)_5$ and the amount of $HNMe_2$ released were found to depend on the number of surface groups generated during the plasma step. At the beginning of the plasma exposure step the molecules $HNMe_2$, CH_4, HCN, and C_2H_2 were measured. After an extended period of plasma exposure, the reaction products CH_4 and C_2H_2 were still present in the plasma. This change in the composition of the reaction products can be explained by an interplay of aspects including the plasma-surface interaction, the ALD surface reactions, and the reactions of products within the plasma. The species formed in the plasma (e.g., CH_x radicals) can re-deposit on the surface and influence to a large extent the TaN_x material composition and properties. © *2012 American Vacuum Society*. [DOI: 10.1116/1.3625565]

I. INTRODUCTION

TaN_x is one of the candidate materials for Cu diffusion barriers and for metal gates in the next semiconductor technology nodes.[1–3] To deposit TaN_x films, atomic layer deposition (ALD) is being investigated with ALD's excellent conformality being of vital interest for the barrier application and ALD's high uniformity and precise growth control being key for the deposition of metal gates.[2,4] TaN_x has many stable and metastable phases ranging from the conductive Ta metal to the semiconductive Ta_3N_5 phase.[5,6] For the deposition of TaN_x, plasma-assisted ALD is considered to be very promising, since a highly reductive environment such as a H_2 plasma is required to obtain the conductive TaN_x phase. However, with the use of H_2 plasma in ALD of TaN, a large variation in composition and resistivity of the films has been reported in the literature.[7–13] To understand the relation between plasma processes and the material properties, a more detailed insight into the reaction mechanism is needed.

In general, there exist only a few reports on reaction mechanism studies of plasma-assisted ALD in the literature. Most of these studies concern O_2-plasma-based processes, i.e., Al_2O_3 (Refs. 14–16), TiO_2 (Ref. 17), and Ta_2O_5 (Ref. 18), and these studies mostly revealed combustionlike reactions during the plasma step. To our knowledge, only one extensive reaction mechanism study has been reported for the growth of metals or metal nitrides by plasma-assisted ALD, which was for the deposition of Ti using $TiCl_4$ and H_2 plasma.[19] For many applications however, metal-organic precursors are preferred to exclude the possibility of introducing halide impurities in the deposited film. Kim *et al.* and Maeng *et al.* speculated on the reaction mechanism during the plasma-assisted ALD process of TaN_x with $Ta(NMe_2)_5$ precursor and H_2 plasma and based their discussion on the TaN_x film composition and on the results for thermal ALD of TiN from $Ti(NMe_2)_4$ and NH_3 (Ref. 9 and 20). They suggested that $HNMe_2$ is released during the precursor step and that $HNMe_2$ and CH_4 are released during the plasma step. Rayner *et al.* proposed a reaction between $Ta(N^tBu)(NEt_2)_3$ at the surface and incoming H radicals (generated by a hotwire source) forming $HNEt_2$ as reaction product.[21] Moreover, it has to be realized that due to the presence of plasma, dissociation and recombination reactions should be considered as they could play an important role in the deposition process.

In this work the reaction mechanism of the plasma-assisted ALD process for TaN_x with $Ta(NMe_2)_5$ precursor and H_2 plasma was investigated by quadrupole mass spectrometry (QMS). The process itself and the material properties obtained were described in our earlier work.[10] First the TaN_x ALD process is briefly reviewed, focusing on changes in the material and process properties with increase in plasma exposure time, i.e., the variation of the material composition, the change in resistivity, and the so-called soft saturation of the growth-per-cycle (GPC). Subsequently, the issues and considerations when using mass spectrometry for studying ALD are discussed and the measurement procedure is described. The aspect of molecule formation in plasmas is considered and illustrated by the observation of NH_3 in

[a)]Electronic mail: w.m.m.kessels@tue.nl

H_2-N_2 plasmas. Using the described measurement procedure, the reaction products during growth of the conductive TaN_x phase were determined. Finally, the reaction mechanisms and growth processes are discussed, addressing the fact that the interaction of the material and the reaction products with the plasma plays an important role in the TaN_x growth process by plasma-assisted ALD.

II. PLASMA-ASSISTED ALD OF TAN_X

In previous publications we reported on the development of a plasma-assisted ALD process for $TaNx$ using PDMAT [$Ta(NMe_2)_5$] and H_2, H_2-N_2, and NH_3 plasmas and showed that the resulting material depended on the plasma composition and the plasma exposure time.[10,11] In short, the remote plasma ALD reactor consisted of a turbomolecular-pumped deposition chamber (base pressure of $< 10^{-5}$ Torr), an inductively coupled plasma (ICP) source, and a precursor dosing system. The plasma source could be separated from the deposition chamber by a gate valve in between. Ar was used as carrier gas at a working pressure of ~30 mTorr to adequately deliver the vapor from the solid $Ta(NMe_2)_5$ precursor which was heated to 75°C. The flow was controlled using a leak valve upstream. The Ar flow was also used for purging the chamber after precursor exposure using a divert line. The remote ICP plasma source was operated at 100 W rf power and 7.5 mTorr pressure of H_2, H_2-N_2, or NH_3 gas. In between the precursor and plasma step the chamber was pumped down ($<10^{-4}$ Torr).

At the typically used ALD exposure times with a 4 s exposure of $Ta(NMe_2)_5$ and 10 s exposure of H_2 plasma at a deposition temperature of 225°C, conductive (1200 $\mu\Omega$ cm), cubic TaN_x films were obtained. By increasing the plasma exposure time to 30 s, the resistivity of the films decreased to 380 $\mu\Omega$ cm. A decrease in deposition temperature had a smaller effect on the resistivity leading to 1300 $\mu\Omega$ cm for depositing at 150°C. Figure 1 shows the change in resistivity and the number of Ta and N atoms deposited per cycle as a function of the plasma exposure time. The resistivity decreases about two orders of magnitude with the increase in plasma exposure time and the material becomes more Ta rich. The number of Ta atoms deposited per cycle increases while the number of N atoms deposited per cycle stays almost constant. Since each Ta atom comes from a $Ta(NMe_2)_5$ precursor molecule, more precursor molecules are apparently adsorbed per cycle when employing longer plasma exposure times. As commonly observed for TaN_x films deposited by ALD, O (~15%) and C (~10%) impurities are present in the films. The O content decreases slightly with plasma exposure time and the O probably originates from precursor impurities and post-deposition oxidation. The C content does not decrease with plasma exposure time and does not show a clear trend. The C content most likely originates from the Me groups in the precursor.

The evolution of the growth-per-cycle (GPC) is considered to better understand the large change in material properties with plasma exposure time. The precursor exposure shows normal saturation behavior (saturating in three seconds) and could be fitted with a single exponential function. The plasma exposure; however, showed a so-called soft saturation behavior characterized by a large increase in GPC in the first few seconds of the plasma exposure and a slow increase over longer time as shown in Fig. 2. Note, that this behavior is not caused by a parasitic CVD growth component, since thermal decomposition of the reactant (H_2 plasma) cannot be an issue. The saturation behavior was fitted with a double exponential function with two time constants.[10] These two time constants basically suggest that two processes play a role, one with a short time constant of 0.7 s, component "a", and one with a long time constant of 8 s, component "b". The two time constants and the accompanying change in material properties can be related to the reaction mechanism of the process and to the reaction products created. The latter will be shown by a systematic QMS study below.

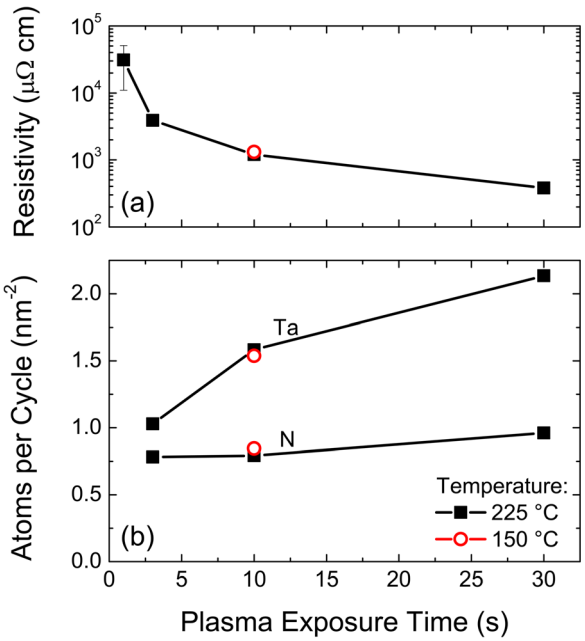

FIG 1. (Color online) Resistivity (a) and the number of Ta and N atoms per cycle per nm^2 (b) for TaN_x deposited by ALD as a function of the H_2 plasma exposure time at a deposition temperature of 225°C. The data for a 10 s plasma exposure at 150°C were included for comparison.

When using plasmas consisting of H_2-N_2 (1:1 ratio) or NH_3, amorphous Ta_3N_5 films with a high resistivity ($\gg 5 \times 10^4$ $\mu\Omega$ cm) and low C content (< 2%) were obtained. Even when only a small amount of N_2 was admixed to the H_2 plasma (98:2 ratio), the N content increased (N/Ta = 1.0) and the resistivity of the films was high (1.1×10^4 $\mu\Omega$ cm). Therefore, the transition to the stable Ta_3N_5 phase is expected to be fast. Consequently, the dependence of the growth process on plasma exposure was not investigated.

III. MASS SPECTROMETRY STUDY FOR ALD

QMS is an excellent tool to study ALD processes. The most prominent merits of QMS are:

(1) The technique is noninvasive. Because only a small amount of gas is extracted in the measurement, the ALD process is not influenced by it.

(2) A relative high time resolution can be obtained when only a few masses are measured at the same time (e.g., 300 ms).
(3) It is easy to interpret when the cracking patterns of the parent molecules are known and/or do not overlap.
(4) It is sensitive as small concentrations of species can be measured especially when the background signals are low.
(5) A wide range of species can be detected, as basically any stable chemical species can be measured. For instance, a sensitive technique such as laser spectroscopy can typically only be used to probe a small selection of molecules due to the typical limited tuning range of the wavelength.

Because of these merits, QMS has been used in a variety of studies of ALD in the literature.[15,18,22–24]

Species detection by QMS occurs as follows: first a small fraction of the gas molecules are extracted from the reactor through the orifice into the QMS and are ionized through electron-impact ionization by electrons with typically an energy of ~70 eV. In typical QMS configurations only stable gas-phase species are detected since plasma radicals, which might be present in the reactor, will generally recombine while entering the QMS, i.e., before they can be ionized. Besides being ionized into parent molecule ions, i.e.,

$$AB + e^- \rightarrow AB^+ + 2e^-,$$

a significant part of the parent molecules will be ionized dissociatively into smaller fragments of the parent molecule:

$$AB + e^- \rightarrow A^+ + B + 2e^-.$$

The parent molecule ions and other ionized fragments will enter the quadrupole mass filter. This mass filter only allows ions within a narrow mass range to pass through on the basis of a properly controlled combination of dc and rf electric fields. The ions that pass through the filter are measured by the SEM detector. It is important to realize that it is not directly the mass of the ionized fragments that is measured, but the mass-to-charge ratio (m/z). Since most fragments have charge one at the used ionization energy of ~70 eV, m/z is in most cases the same as the mass of the ion. The mass spectrum resulting from the fragmentation of a particular molecule is referred to as the cracking pattern. The cracking pattern is a kind of fingerprint of the molecule and can be used to identify the parent molecules responsible for a measured spectrum. The NIST database can be used which contains a wide range of cracking patterns from a variety of sources.[25] However, it should be realized that QMS setups can vary greatly in their sensitivity as a function of the m/z value depending on the configuration and on the parameter settings.

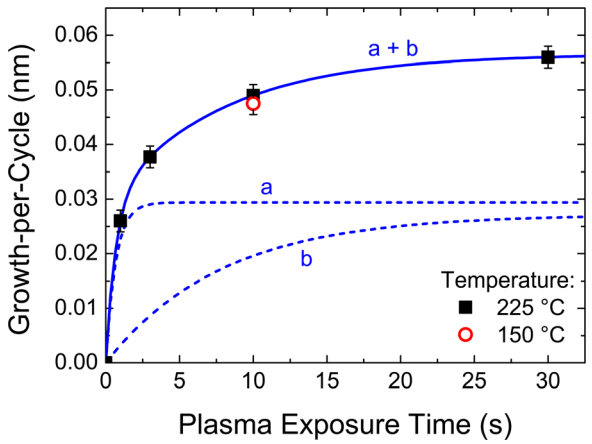

FIG 2. (Color online) Growth-per-cycle for TaN_x as a function of the plasma exposure time at a deposition temperature of 225°C. The solid line shows the double exponential decay fit with two time constants. The two contributions (a) and (b) with different time constants are shown separately in dashed lines. The growth-per-cycle for 10 s plasma exposure at 150°C was included for comparison.

When following several m/z ratios, the time per m/z measurement is determined by the dwell time and the delay time. The dwell time is the time over which the SEM detector signal is integrated (e.g., 50 ms); the delay time is the dead time for changing between m/z values. The delay time should be sufficiently long for the mass filter to stabilize at a certain setting (e.g., 10 ms). Otherwise, also fragments other than those with the target m/z value will contribute to the signal. Moreover, it is advisable to measure m/z values in an order from low to high to minimize the magnitude of the changes in m/z value setting. When measuring from low to high m/z values contributions from fragments at unwanted m/z values can be avoided. Besides that, so-called pressure effects can also be present, i.e., changes in signal due to changes in pressure even when the measured signal is not from a species causing the pressure change. Therefore, comparison of signals should be done at similar reactor pressures. Furthermore, because the sensitivity of the QMS can vary over time, reference signals should be used to correct for this variation when different measurements have to be compared. For example a signal from Ar^+ ($m/z = 40$) can be chosen as reference signal. In this case a known partial pressure of Ar gas should be present during the ALD process.

A. QMS measurement procedure

The QMS can operate in different modes, either measuring a wide mass range (e.g., $m/z = 1 - 100$) with low time resolution (also referred to as a mass scan) or a few masses with higher time resolution (also referred to as a time-dependent scan). The stepwise nature of ALD and the associated short time in which reaction products are released require a carefully considered measurement procedure to determine the reaction products. Measuring a large range of masses is desired to unambiguously attribute changes at certain m/z values to specific gaseous species. However, to achieve sufficient time resolution, the time resolved measurements should be carried out by monitoring only a few m/z values at the same time. Due to the cyclic nature of ALD in which the process is continuously repeated, the measurements at different m/z values during different cycles can be combined to form a mass spectrum for a single cycle. This

mass spectrum represents the signals during a single cycle for of a wide range of masses with a high time resolution. To improve the signal-to-noise ratio the signals of multiple cycles can be used for averaging and the reference signal can be used to monitor the reproducibility of the measurements. To distinguish the signals caused by reaction products from the background signals properly chosen reference spectra are measured. Reaction products will not be formed when the surface reactions are already saturated so repeating a precursor or reactant exposure under saturated conditions will show their cracking patterns and can therefore serve as a reference. When plasma is used as reactant, a measurement under zero plasma power yields the signal for only the source gasses.

For the QMS measurements, a differentially-pumped quadrupole mass spectrometer (Pfeiffer QME 200, mass-to-charge ratio $m/z = 0 - 200$) with a 150 μm orifice was fitted to the side of the reactor. In the measurement procedure for the TaN_x process, four m/z values were measured at the same time. The measurement per four m/z values consisted of five normal ALD cycles ("normal ALD"), five cycles with zero plasma power ("precursor only"), and five cycles with no $Ta(NMe_2)_5$ ("plasma only"). The "plasma only" cycles were performed by keeping the precursor valves closed (the Ar flow is not diverted through the $Ta(NMe_2)_5$ bubbler), and the "precursor only" cycles were performed by setting the plasma power to zero in the cycle. Therefore both "cycle conditions" have basically the same pressure changes as a normal cycle minimizing any "pressure effects" in the signal. The measurement per four m/z values was repeated until data were obtained for all m/z ratios in the range of $m/z = 12 - 46$. In each measurement, the signal at $m/z = 40$ (Ar^+) was included to serve as a reference while the other three m/z values varied. On the basis of the Ar^+ signal, the different measurements were synchronized afterwards. Furthermore, the signal at $m/z = 40$ (Ar^+) during the precursor step was used to monitor the sensitivity of the QMS and was used to normalize the signal. The signal at each m/z value for each "cycle condition", i.e., "normal ALD", "precursor only", and "plasma only", was averaged over the last four cycles as the first cycle typically showed influences from the previous "cycle condition".

Figure 3 shows the contributions in the QMS signal for the precursor and plasma step measured during the three "cycle conditions". In this case $m/z = 15$ is used as an example. During the "normal ALD" cycle the precursor step has contributions from cracking of $Ta(NMe_2)_5$ precursor, from reaction products formed in ALD surface reactions, and from background signals including the Ar flow. The plasma step has contributions from plasma gas species, from reaction products and from background signals including the H_2 flow. The "precursor only" and "plasma only" cycles represent situations for which extended $Ta(NMe_2)_5$ exposure or extended plasma exposure times have been employed, respectively. In the case of an extended $Ta(NMe_2)_5$ exposure time no contribution by reaction products is expected due to saturation of the precursor adsorption. Normally, also in the case of extended plasma exposure times no new reaction products are expected. However, due to the plasma-surface

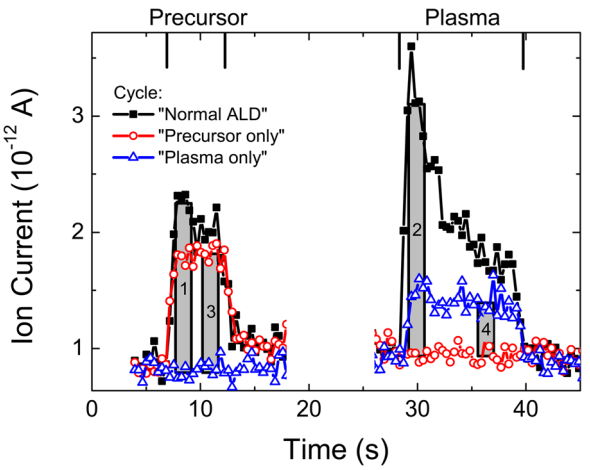

FIG 3. (Color online) Averaged ion current for $m/z = 15$ as a function of time for the "normal ALD" cycle, the "precursor only" cycle, and the "plasma only" cycle. The vertical bars with numbers 1 to 4 indicate the signals used to construct the combined spectra with multiple masses (Figs. 7–9). The precursor exposure and plasma exposure durations are indicated at the top of the figure.

interaction, processes that cause a change in material properties can release gas-phase products. The reaction products for the $Ta(NMe_2)_5$ and plasma step can therefore be determined by comparing the signals measured during the "normal ALD" cycle with the signals for the cycles where either the $Ta(NMe_2)_5$ exposure or the plasma exposure was omitted. Possible reaction products after extended plasma exposure can be determined by comparing the plasma step of the "plasma only" cycle with the plasma step of the cycle with zero plasma power ("precursor only"). To be able to get a good overview of all the data, four mass spectra were constructed using all m/z values. In Fig. 3 the signals used for the mass spectra are indicated for $m/z = 15$ with vertical bars. Two mass spectra represent the signal for the reaction products during the precursor step (signal 1) and during the plasma step (signal 2) in the ALD cycle, while the other two mass spectra represent the reference signals which are the situations after extended precursor exposure (signal 3) or after extended plasma exposure (signal 4).

It should be noted that surface-generated species measured in the QMS can originate from all surfaces. Since reactor wall surfaces are typically large compared to the substrate size, species from the wall can contribute to a large extent to the measured signal. To ensure that all measured reaction products originate from reactions at the same temperature, both the wall and substrate temperature should be set to the same temperature. In this study the temperatures were set to 150°C. Therefore, reactions are representative for ALD growth of TaN_x at 150°C, which is fairly similar to ALD growth of TaN_x at 225°C as shown by the data in Figs. 1 and 2.

IV. RESULTS AND DISCUSSIONS

A. Dissociation and formation of molecules in plasmas

H_2 and N_2 plasmas are often used in plasma-assisted ALD since they generate H and N radicals. However, plasma

radicals can recombine and therefore H_2–N_2 plasmas can also produce species such as NH_3. Although dissociation reactions involving two species can occur in the gas phase at the pressures typically employed during plasma ALD, three body reactions in the gas phase are more unlikely and most of the molecule formation will therefore occur at surfaces.[26] The formation of NH_3 will occur according to the net conversion reaction:

$$N_2 + 3\,H_2 \leftrightarrow 2\,NH_3.$$

Obviously, species generated by the plasma can again be dissociated and NH_3 dissociation can therefore lead to NH and NH_2 radicals.

To study the molecule formation in H_2, H_2-N_2, and NH_3 plasmas, three mass spectra were measured for each plasma: (1) the mass spectrum during plasma operation ("plasma on"); (2) the mass spectrum of the plasma gas mixture ("plasma off"); and (3) the mass spectrum with the reactor at base pressure. The mass spectrum with the reactor at base pressure shows the baseline due to residual species in the reactor chamber and mass spectrometer.

As expected, in pure H_2 plasmas no molecules other than H_2 are produced. Figure 4 shows the mass spectrum of a H_2-N_2 (1:1) gas mixture for the "plasma on" and "plasma off" case. Also the base signal level is indicated. The base pressure spectrum shows the presence of H_2O in the background through its cracking pattern at $m/z = 16$, 17, 18. Comparing the mass spectrum of the "plasma off" case with the base spectrum, an increase in the masses for H_2 ($m/z = 2$) and N_2 ($m/z = 7$, 14, 28) is observed as expected. A comparison between the "plasma on" and "plasma off" case shows an increase for $m/z = 15$, 16, and 17. These m/z values and the relative intensities at which they are observed correspond with the cracking pattern of NH_3, indicating the formation of NH_3 in the H_2-N_2 plasma. The accompanied decrease of H_2 and N_2 is only small (especially on the logarithmic scale). This implies that only a small fraction of these molecules are converted in NH_3.

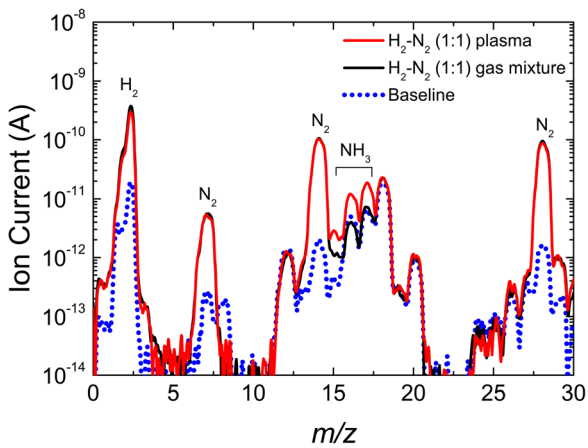

FIG 4. (Color online) Mass spectra measured for: a H_2-N_2 plasma (1:1), a H_2-N_2 gas mixture (1:1), and with the reactor at base pressure. The main parent molecules of the fragments are indicated.

To investigate the amount of NH_3 formed in the H_2-N_2 plasma, the NH_3 m/z signals were calibrated by introducing gas mixtures with known partial pressures of NH_3 in the reactor. The volume fraction of NH_3 was varied and the total pressure was kept constant at the same value used for the other measurements to minimize any "pressure effects." With these known partial pressures for NH_3, the relations between the measured ion currents at $m/z = 16$ and 17 and the partial pressure were determined. Using this calibration the volume fraction of NH_3 in the plasma was calculated.

Figure 5 shows the volume fraction of NH_3 in an H_2-N_2 plasma as a function of the volume fraction of H_2 with respect to the total H_2-N_2 gas mixture. All volume fractions are expressed as a percentage of the original gas mixture. The maximum in NH_3 production is obtained at around 60% H_2 resulting in about 4% of NH_3. Our results relate well to a similar study by Van Helden *et al.* on expanding thermal plasma reactors (with different geometries and volumes), the maximum in NH_3 production was found to occur in the same range, i.e., 60% – 70% H_2, and had the same magnitude, i.e., 2% – 10% NH_3 produced.[27]

Instead of a H_2-N_2 plasma also an NH_3 plasma can be employed during ALD. When employing such plasma, a large part of the NH_3 is dissociated into H_2 and N_2 which leads to an increase in the total number of particles. Corresponding to the net conversion reaction it was found that roughly 40% of the NH_3 is dissociated, giving 60% H_2 and 20% N_2. Together with the remaining 60% NH_3 this reveals that the particle number density increases to 140% of the initial amount. This is in rough agreement with the observed pressure increase to 170% of the initial pressure. The difference is likely caused by heating of the gas.

As addressed earlier, both the use of H_2-N_2 and NH_3 plasmas in ALD of TaN_x basically result in the same material, Ta_3N_5. This is not surprising considering the fact that these plasmas have similar compositions, i.e., a combination of H_2, N_2, NH_3, and N_xH_y radicals. Although the relative

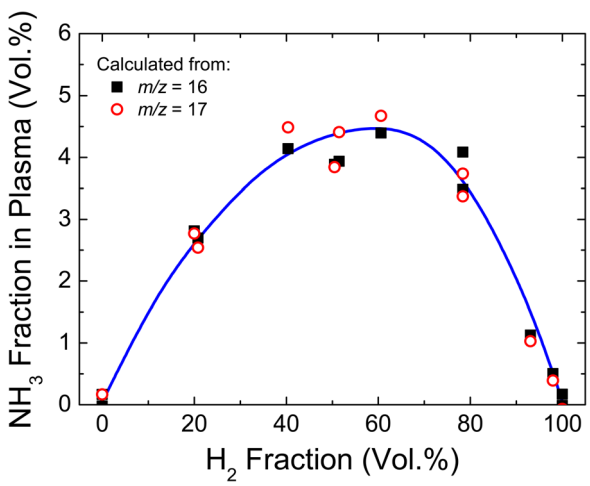

FIG 5. (Color online) NH_3 production in a H_2-N_2 plasma as a function of the volume fraction of H_2 with respect to the total H_2-N_2 gas mixture. The NH_3 amounts were calculated from the $m/z = 16$ and 17 signal measured by the QMS. The percentages are given with respect to the original H_2-N_2 gas mixture.

concentrations of these species will be different in these plasmas, this apparently does not significantly affect the resulting material composition. When discussing the reaction mechanisms during the plasma step it will be shown that molecule formation can also occur using pure H_2 plasmas when ALD reaction products are released from the surface.

B. Cracking pattern of $Ta(NMe_2)_5$

The cracking pattern of the $Ta(NMe_2)_5$ precursor was determined to be able to distinguish signals due to the precursor from signals due to reaction products. An Ar flow was used to transport the $Ta(NMe_2)_5$ into the chamber in the same way as during the precursor exposure step in the ALD cycle. To determine the cracking pattern of $Ta(NMe_2)_5$, the spectrum for pure Ar measured at the same pressure was subtracted from the $Ta(NMe_2)_5 + Ar$ spectrum. Fragments containing Ta were not detected, most probably due to the reduced sensitivity of the QMS in the high m/z range ($m/z = 181$ for Ta^+). Figure 6 shows the $Ta(NMe_2)_5$ cracking pattern. The $HNMe_2$ pattern from the NIST database is included for comparison.[25] The two spectra show good overlap in the m/z values. Violet *et al*. have shown that during mass spectrometry of $Ta(NMe_2)_5$, fragments from the molecule $HNMe_2$ are measured,[28] which explains the agreement between the cracking pattern of $Ta(NMe_2)_5$ and $HNMe_2$ in this mass range. They suggested that $HNMe_2$ is formed in the mass spectrometer by NMe_2 detachment from $Ta(NMe_2)_5$ and subsequent reaction of the detached NMe_2 with hydrogen adsorbed on the mass spectrometer walls.[28] Assuming that also in the present case the $Ta(NMe_2)_5$ cracking pattern is dominated by $HNMe_2$-related species, the observed intensity difference between the experimental $Ta(NMe_2)_5$ and the NIST $HNMe_2$ spectrum as a function of m/z value can be explained by a difference in sensitivity and/or transmission for different m/z values, as often observed for different QMS systems in the literature.[29] The signal at $m/z = 17$ and 18 can be attributed to fluctuations in the H_2O levels present in the background during the measurements.

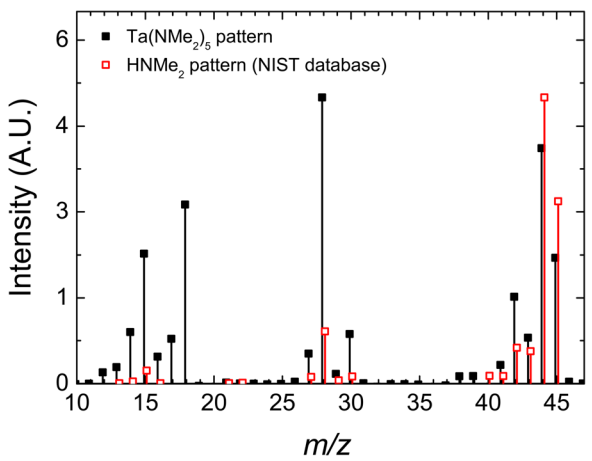

FIG 6. (Color online) $Ta(NMe_2)_5$ cracking pattern measured at 70 eV electron energy. The cracking pattern was obtained by subtracting the Ar spectrum from the $Ta(NMe_2)_5 + Ar$ spectrum. A comparison is made with the $HNMe_2$ cracking pattern taken from the NIST database. Small mass offsets in m/z values on the horizontal axis ($\Delta m/z = 0.1$) are introduced for clarity.

C. Reaction products: precursor step

In Fig. 7, the spectra during $Ta(NMe_2)_5$ exposure for a "normal ALD" cycle (signal 1 in Fig. 3) and for a "precursor only" cycle (signal 3 in Fig. 3) are shown. The spectrum during a "normal ALD" cycle is the result of cracking of $Ta(NMe_2)_5$ and cracking of reaction products, and the spectrum during a "precursor only" cycle is the result of $Ta(NMe_2)_5$ cracking only. Interestingly, the m/z values at which a signal is observed are the same for the two spectra. This can be explained by a main contribution to the signals by $Ta(NMe_2)_5$ and $HNMe_2$ for the "normal ALD" cycle since the cracking pattern for $HNMe_2$ is very similar to the cracking pattern for $Ta(NMe_2)_5$ in this m/z range as shown in Fig. 6 (Ref. 28). The spectrum intensity level cannot be explained by precursor cracking only because the measured intensity for the "normal ALD" cycle is higher than for the $Ta(NMe_2)_5$ spectrum. Therefore, it can be concluded that $HNMe_2$ is present as a reaction product. The resulting intensities of the signals during ALD are therefore a combination of $Ta(NMe_2)_5$ which is partially consumed and $HNMe_2$ which is produced. The amount of $HNMe_2$ produced per consumed $Ta(NMe_2)_5$ could be quite high since in the literature it has been reported that for thermal ALD most of the ligands are released during the precursor adsorption. For ALD with $Ta(N^tBu)(NEt_2)_3$ and N_2H_4 it was reported that three out of four ligands were removed during precursor adsorption.[30] However, no quantitative conclusions on the number of ligands released can be drawn from the intensity difference. For example, the higher measured intensity level in this m/z range could be simply due to a relatively higher signal per measured $HNMe_2$ molecule than the signal per measured $Ta(NMe_2)_5$ molecule. For instance, ionization of

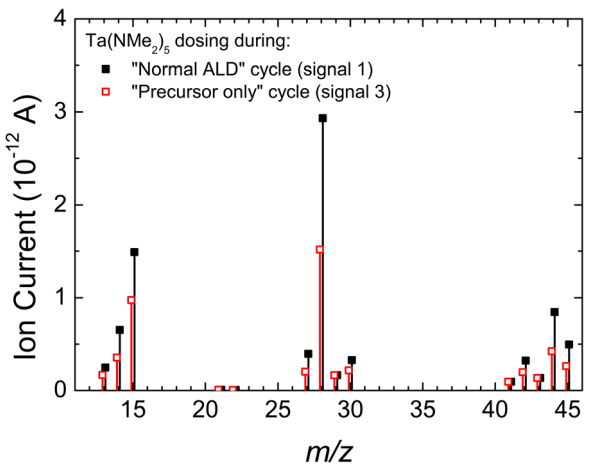

FIG 7. (Color online) Mass spectrum during $Ta(NMe_2)_5$ exposure for a "normal ALD" cycle and for a "precursor only" cycle. The spectra were constructed by combining the signal intensities for the different m/z values as described in the measurement procedure section. The intensities from signals 1 and 3 were determined as illustrated for $m/z = 15$ in Fig. 3 Small mass offsets in m/z values on the horizontal axis ($\Delta m/z = 0.1$) are introduced for clarity.

$Ta(NMe_2)_5$ could in principle result predominantly in ionized fragments containing Ta which would have higher masses and would cause a relative low intensity for $Ta(NMe_2)_5$ in the measured m/z range.

D. Reaction products: plasma step

Figure 8 shows the mass spectrum representing the reaction products during the beginning of the plasma step (signal 2 in Fig. 3). The spectrum can be accounted for by a combination of cracking patterns representing different molecules. The used cracking patterns represent the following molecules: $HNMe_2$, CH_4, C_2H_2, and HCN. Cracking patterns that span a wide m/z range such as the cracking pattern for $HNMe_2$ show more difference between different QMS setups and therefore it is better to use a cracking pattern obtained using the same QMS setup than to use the one from the NIST database. To this end, the measured $Ta(NMe_2)_5$ cracking pattern (signal 3 in Fig. 3) can be used as a cracking pattern for $HNMe_2$ as discussed in the previous section. The cracking patterns for CH_4, C_2H_2, and HCN were obtained from the NIST database.[25] The cracking patterns were scaled such that their linear combination roughly corresponds with the measured spectrum. Due to the high background of H_2O in the QMS only large signals can be detected at $m/z = 17$ and 18. Therefore, small amounts of H_2O and/or NH_3 as reaction product could be present, despite the fact that no clear difference in signal was observed at these m/z values. The respective levels of $C_2H_2^+$ at $m/z = 26$ and HCN^+at $m/z = 27$ were about equal in the linear combination used. This implies that the concentrations of C_2H_2 and HCN are roughly similar, since the ionization cross-sections of C_2H_2 to $C_2H_2^+$, and HCN to HCN^+, are expected to be similar as in both cases it concerns ionization of the parent molecule without dissociation.

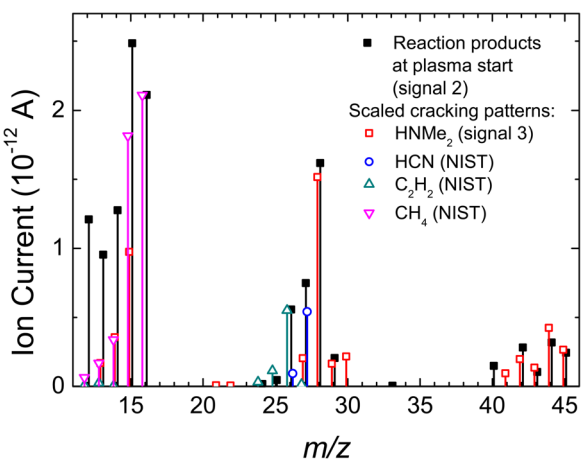

FIG 8. (Color online) Spectrum showing the reaction products during the beginning of the H_2 plasma (signal 2). Cracking patterns from the NIST database and the measured cracking pattern for $HNMe_2$ (signal 3) are scaled to account for the measured spectrum. The spectra for signals 2 and 3 were constructed by combining the signal intensities for the different m/z values as described in the measurement procedure section. The intensities for signals 2 and 3 were determined as illustrated for $m/z = 15$ in Fig. 3 Small mass offsets in m/z values on the horizontal axis ($\Delta m/z = 0.1$) are introduced for clarity.

Figure 9 shows the spectrum of the reaction products during the beginning of the plasma step, and the spectrum after extended plasma exposure. After extended plasma exposure a few signals which were also present at the beginning of the plasma are still observed. These are the signals which can be attributed to CH_4 and C_2H_2. Apparently, these products are present in the plasma for a longer time (roughly equivalent to 30 s plasma exposure). Although the signal for C_2H_2 at m/z values 24, 25, and 26 is low, the signal can be clearly distinguished due to the low background signals at these m/z values.

E. Reaction products: time dependence

Apparently, besides a decrease in reaction product concentration during the plasma exposure due to the reaching of saturation also the composition of the reaction products changes over time. To obtain more insight into this time dependence a few specific masses were followed during an extended plasma exposure time. Furthermore, optical emission spectroscopy (OES) was used to measure emission from excited species in the plasma. Optical emission spectroscopy measurements were carried out by measuring the plasma emission just above the substrate holder by using an Ocean Optics USB2000 spectrometer.[31] Besides emission from excited H and H_2 species, the emission from CN radicals was observed.[10,31] The excited CN radical can for example be produced from HCN by the following reaction:

$$HCN + e^- \rightarrow CN + H + e^-.$$

Note, that although no emission from CH_x and NH_x radicals was observed, these radicals were expected to be present as well. CH_x and NH_x radicals might simply not be excited to energy levels resulting in optical emission. Figure 10 shows the CN emission at 388 nm and the QMS signal at $m/z = 15$, 27, and 45 for three subsequent plasma exposures. For the

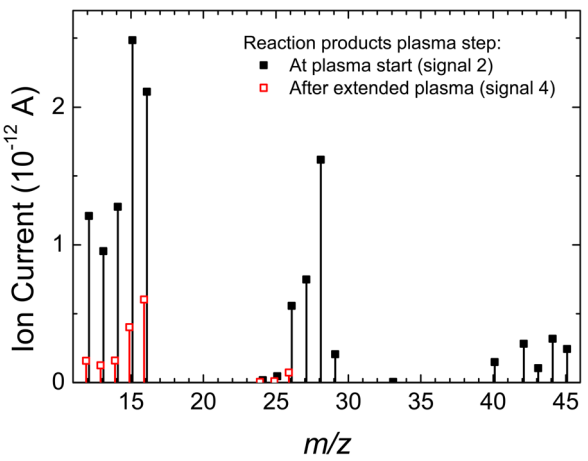

FIG 9. (Color online) Spectrum showing the reaction products during the beginning of the H_2 plasma and during an extended H_2 plasma exposure of ~30 s. The spectra were constructed by combining the signal intensities for the different m/z values as described in the measurement procedure section. The intensities from signals 2 and 4 were determined as illustrated for $m/z = 15$ in Fig. 3 Small mass offsets in m/z values on the horizontal axis($\Delta m/z = 0.1$) are introduced for clarity.

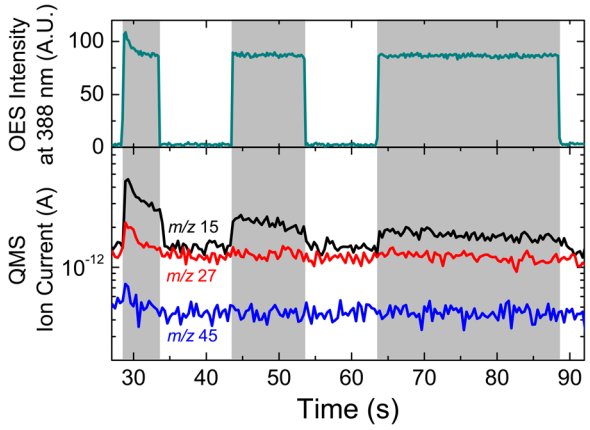

FIG 10. (Color online) Extended H_2 plasma exposure after a precursor exposure step. The plasma exposure is interrupted twice. The plasma emission at 388 nm was measured with OES, and the *m*/*z* values 15, 27, and 45 were monitored by QMS. The periods with the plasma power applied are indicated in gray.

first plasma exposure, power was applied for 5 seconds followed by a 10 s interruption. This was followed by a second plasma exposure by applying power for 10 s, again a 10 s interruption and finally an exposure by applying power for 25 seconds. In total the plasma exposure was therefore 40 s. All lines have a higher intensity at the start of the first plasma exposure after the $Ta(NMe_2)_5$ exposure. This is not a plasma start-up effect since this effect is not present for the second and third plasma exposure step. As was shown in the previous section, during this initial period the reaction products $HNMe_2$, CH_4, C_2H_2, and HCN were present in the gas phase. The intensity increase in OES emission shows that also excited CN was present. The OES emission at 388 nm and the QMS signals at *m*/*z* values 27 and 45 decreased quickly to the background level after the first plasma exposure and could no longer be distinguished from the background level. The signal for $m/z = 15$ was visible during the full plasma exposure time and shows that CH_4 continued to be present in the gas phase during these exposures. The continuation of the $m/z = 15$ signal at the same height after the purging between the plasma exposures leads to the conclusion that the CH_4 is a product of plasma-surface interactions. If the CH_4 was originating from a gas-phase reaction involving residual reaction products in the gas phase, the intensity should be lower after purging.

Similar to the two timescales present in the soft saturation behavior of the GPC, there seem to be two timescales present in the decay of the reaction products. Fitting an exponential decay to the OES signal reveals that it has a similar timescale as the fast process in Fig. 2 (time constant is 0.8 s compared to 0.7 s). Although the signal for $m/z = 15$ is quite noisy, the signal can be fitted with a single exponential decay function to obtain a time constant for the process with the long timescale. Although the accuracy of the data does not allow a precise comparison, the resulting time constant (~16 s) and the long time constant in Fig. 2 (8 s) are both in the order of 10 s. Note that the data in Fig. 2 refer to a "local" measurement (ellipsometry on the substrate) whereas the data in Fig. 10 refer to a "global" measurement (mass spectrometry probing the species present in the whole reactor). Nonetheless, the similarity between the time constants might indicate a relation between the processes which are responsible.

V. DISCUSSION ON THE REACTION MECHANISMS

Reaction mechanisms taking place during plasma-assisted ALD of TaN_x using $Ta(NMe_2)_5$ and H_2 plasma can be postulated by considering the measured reaction products and by considering the dependence of the material properties on plasma composition and exposure. The main observations by QMS are:

(1) During the $Ta(NMe_2)_5$ exposure step, the reaction product $HNMe_2$ is detected
(2) During the plasma exposure step, immediately after striking the plasma, the molecules $HNMe_2$, CH_4, C_2H_2, and HCN are measured. After an extended plasma exposure time the reaction products CH_4 and C_2H_2 are still observed in the plasma.

These observations can be related to the dependence of the TaN_x material properties on plasma exposure time shown in Figs. 1 and 2.

A. $Ta(NMe_2)_5$ exposure

The incoming precursor adsorbs by reacting with H at the surface. The reaction between an x number of surface species containing H and precursor ligands results in the formation of an x number of $HNMe_2$ molecules:

$$x\ \text{surf-H} + \text{Ta}(\text{NMe}_2)_5 \rightarrow \text{surf-Ta}(\text{NMe}_2)_{5-x} + x\ \text{HNMe}_2.$$

The reactive hydrogen at the surface is most likely present in the form of $-NH_x$ and $-TaH$. Also the presence of $-OH$ from O impurities cannot be excluded. Hydrogen in the form of $-CH_x$ is expected to be unreactive towards the precursor. Whether the ligands are removed directly during adsorption or by hydride elimination reactions after adsorption,[30] cannot be concluded from the present data.

To estimate how many ligands are removed per precursor molecule (x), the maximum amount of ligands on the surface due to steric hindrance is first estimated. To this end the GPC for the Ta_2O_5 process using $Ta(NMe_2)_5$ and O_2 plasma is considered.[18] For this process, the GPC does not change in the temperature window, which suggests that kinetic processes are not the limiting factor. Furthermore, the constant GPC suggests that additional hydroxylation or dehydroxilation processes do not play a significant role since those would also be temperature-dependent processes. Therefore, the assumption can be made that steric hindrance determines the GPC in this case. Another assumption is that during the reactant step for each removed ligand one new surface group is created on which a ligand can adsorb in the next half-cycle.[32] Together with the fact that the precursor is homoleptic, this assumption leads to the conclusion that the average amount of ligands on the surface after precursor adsorption is 2.5 per precursor molecule (i.e., half of the ligands). Assuming that the precursor adsorption per cycle is

equivalent to the amount of Ta deposited per cycle, the number of adsorbed precursor molecules for Ta_2O_5 becomes 1.8 nm^{-2} (Ref. 18). With 2.5 ligands remaining per adsorbed precursor molecule, a saturated coverage of NMe_2 ligands of 4.5 nm^{-2} can be calculated.

The number of precursor molecules adsorbed for the TaN_x process with 30 s plasma is 2.1 nm^{-2} as indicated in Fig. 1. If 2.5 ligands would remain per adsorbed precursor, the NMe_2 coverage would be higher than the maximum coverage due to steric hindrance reasons as just calculated (5.3 versus 4.5 nm^{-2}). This suggests that more than 2.5 ligands have to be removed during precursor adsorption ($x > 2.5$). This implies, therefore, that to remove these ligands additional surface groups have to be created during the 30 s plasma exposure besides the ones created for each removed ligand. Similar conclusions have been drawn for Al_2O_3 at low temperature, where additional OH groups are created resulting in removal of more than 1.5 ligands (i.e., half of the total number of ligands of $AlMe_3$) during $AlMe_3$ adsorption.[33] Burton *et al.* also suggested that more than half of the ligands are removed for thermal ALD of TaN using $Ta(N^tBu)(NEt_2)_3$ and N_2H_4. They also suggested creation of additional surface groups for precursor adsorption during the reactant step.[30]

B. H_2 plasma exposure

Unlike the reaction products during the precursor step, not all detected molecules in the plasma have to be directly related to ALD reactions. Molecules created through surface reactions, which enter the plasma, can be dissociated by electron impact dissociation, leading to the formation of reactive fragments of the molecules (i.e., radicals) and the generation of new molecules. This dissociation of reaction products has also been observed in plasma-assisted ALD using O_2 plasmas where CO_2 can be dissociated by the plasma into CO (Ref. 15). Due to the low pressure and the associated unlikelihood of three-body reactions in the gas phase, recombination of the plasma radicals into new molecules will mostly occur at surfaces. $HNMe_2$ is expected to be a direct product of ALD reactions, but the other products (CH_4, C_2H_2, and HCN) can also be formed by the dissociation of $HNMe_2$ in the plasma and subsequent surface-mediated molecule formation from the fragments.

Ta is in the 5+ oxidation state in the precursor and has to be reduced to the 3+ oxidation state to form conductive TaN. H radicals can reduce the Ta atom, and react with the NMe_2 surface groups to form $HNMe_2$:

$$H + Ta^{5+} \rightarrow H^+ + Ta^{4+},$$

$$H^+ + \text{surf} - NMe_2^- \rightarrow HNMe_2.$$

For these reactions also the oxidation state has to be taken into account, since the oxidation state changes during the plasma step. If the growth process only consists of the removal of complete ligands by H radicals, the resulting material from the plasma-assisted ALD process should be pure Ta metal. However, TaN_x is deposited with N being one of the major constituents of the film. Removal of the Me groups by CH_4 formation has been proposed as a reaction leading to N in the film:[9,13,20]

$$4\,H + \text{surf} - NMe_2^- \rightarrow \text{surf} - NH_2^- + 2\,CH_4.$$

The $HNMe_2$ and CH_4 reaction products can decompose in the plasma leading to formation of CH_4, C_2H_2, HCN, and their radicals. The formed molecules and radicals can be pumped away or can re-deposit on the surface forming new surface groups (e.g., $-NH_x$ and $-CH_x$). The radicals have different sticking probabilities on the surface. Liu *et al.* reported that the respective sticking probabilities of CH, CN, NH_2, and NH decrease from very high (~1) to low (~0.1) (Ref. 34). The variation in the sticking probabilities corresponds with the observed change over time in reaction product composition during the plasma exposure. Initially, species containing N, C, and H are observed ($HNMe_2$, HCN, CH_4, and C_2H_2), while with the increase in plasma exposure time the species containing only C and H dominate as reaction product (CH_4 and C_2H_2). The lower sticking probability of species containing N, facilitates the removal of these species from the reactor once N is removed from the film, which also corresponds with the decrease of the N/Ta ratio with increase in plasma exposure time shown in Fig. 1(b). In contrast, the "sticky" CH_x radicals redeposit more easily and lead to an extended presence of species containing C, which in turn corresponds with the observed presence of C in the deposited film. Also stable species can have a relatively high sticking probability (e.g., for C_2H_2 a unity sticking probability has been reported on Ta surfaces[35]). Note that studies of the sticking probability of CH_3 radicals on carbon films have revealed a very low sticking probability; however in the presence of a H radical flux or ion bombardment, as is the case during the plasma exposure step, the CH_3 sticking probability is reported to increase strongly.[36,37]

The lack of detection of more hydrogen rich C_2H_x species can be explained by the fact that C_2H_4 dehydrogenates to C_2H_2 on Ta surfaces.[35] Note that C_2H_2 formation from CH_4 is known in plasmas.[38,39] Small amounts of CH_4 in H_2 plasmas are furthermore known to influence the material properties by forming the TaC phase and free carbon in the case of plasma-assisted ALD of TaC_xN_y using a H_2-CH_4 plasma.[40] The low resistivity observed at extended plasma exposures could be related to the presence of inclusions of the conductive TaC phase.[41]

Towards the end of the plasma exposure probably no intact NMe_2 ligands are present and the surface is covered by CH_x, NH_x, and H species. During this period of the plasma exposure, the observed CH_4 can no longer come from $HNMe_2$ dissociation but has to originate from other surface groups. The change in surface groups could be related to the fast and slow process observed in the GPC in Fig. 2. Another explanation for the "soft" saturation could be that it becomes more difficult to remove surface groups as the oxidation state of Ta decreases. In our earlier paper we suggested a different interpretation in which the short timescale relates to the removal of ligands and the long time constant relates to the change in material properties.[10] Although this interpretation is different from the ones proposed in this

paper the interpretations do not conflict with each other. To determine the exact reaction pathways and confirm the suggested mechanisms, sensitive *in situ* surface diagnostics such as infrared spectroscopy would be needed.

To summarize, in the plasma step the reaction products can be dissociated in the plasma and the dissociated products can redeposit and influence the ALD growth process. Because these plasma reactions and redeposition processes differ for different species, the composition of the reaction products can change in time for the plasma step. This knowledge can be used to optimize the ALD process. For instance, by decreasing the residence time of the gas in the reactor the interaction of the reaction products with the plasma can be reduced. Another possibility would be on-off modulation of the plasma on the time scale of the residence time.

VI. CONCLUSIONS

The reaction mechanisms of plasma-assisted atomic layer deposition (ALD) of TaN_x using $Ta(NMe_2)_5$ precursor were studied using quadrupole mass spectrometry (QMS). Molecule formation in plasmas was addressed and exemplified by the formation of 4% NH_3 in a H_2-N_2 (1:1) plasma.

From the QMS measurements the reaction products during growth of the conductive TaN_x using a H_2 plasma were determined. During $Ta(NMe_2)_5$ exposure the reaction product $HNMe_2$ was detected, which can be attributed to the reaction of $Ta(NMe_2)_5$ with the surface groups generated during the plasma. The amount and/or kind of surface groups generated during the plasma exposure determines the amount of precursor adsorbed.

At the beginning of the plasma exposure step the molecules $HNMe_2$, CH_4, C_2H_2, and HCN are measured, while after extended plasma exposure time only the reaction products CH_4 and C_2H_2 were observed. This change in the composition of the reaction products was related to the reaction mechanisms taking place on the surface and in the plasma. $HNMe_2$ and CH_4 can be formed by the reaction of H radicals with the NMe_2 ligands at the surface. These products interact with the plasma such that also HCN and C_2H_2 are formed. The fact that CH_x radical species have a higher sticking probability is expected to explain the extended presence of CH_4 and C_2H_2 in the plasma. In general, it can therefore be concluded that the material composition and properties are determined to a large extent by the plasma-surface interaction and by the reactions of products with the plasma.

ACKNOWLEDGMENTS

S.E. Potts is acknowledged for the insightful discussions. This work was sponsored by the Materials innovation institute M2i (www.m2i.nl) under project number MC3.06278. This work was supported by the Dutch Technology Foundation STW.

[1]*International Technology Roadmap for Semiconductors*, 2009 ed., www.itrs.net.
[2]H. Kim, Surf. Coat. Technol. **200**, 3104 (2006).
[3]K. S. Chang, M. L. Green, I. Levin, J. R. Hattrick-Simpers, C. Jaye, D. A. Fischer, I. Takeuchi, and S. De Gendt, Appl. Phys. Lett. **96**, 192114 (2010).
[4]R. Sreenivasan, T. Sugawara, K. C. Saraswat, and P. C. McIntyre, Appl. Phys. Lett. **90**, 102101 (2007).
[5]C. Stampfl and A. J. Freeman, Phys. Rev. B **67**, 064108 (2003).
[6]C. Stampfl and A. J. Freeman, Phys. Rev. B **71**, 024111 (2005).
[7]J. S. Park, M. J. Lee, C. S. Lee, and S. W. Kang, Electrochem. Solid-State Lett. **4**, C17 (2001).
[8]J. S. Park, H. S. Park, and S. W. Kang, J. Electrochem. Soc. **149**, C28 (2002).
[9]H. Kim, C. Detavenier, O. van der Straten, S. M. Rossnagel, A. J. Kellock, and D. G. Park, J. Appl. Phys. **98**, 014308 (2005).
[10]E. Langereis, H. C. M. Knoops, A. J. M. Mackus, F. Roozeboom, M. C. M. van de Sanden, and W. M. M. Kessels, J. Appl. Phys. **102**, 083517 (2007).
[11]H. C. M. Knoops, L. Baggetto, E. Langereis, M. C. M. van de Sanden, J. H. Klootwijk, F. Roozeboom, R. A. H. Niessen, P. H. L. Notten, and W. M. M. Kessels, J. Electrochem. Soc. **155**, G287 (2008).
[12]C. Hossbach *et al.*, J. Electrochem. Soc. **156**, H852 (2009).
[13]Q. Xie, D. Deduytsche, J. Musschoot, R. L. V. Meirhaeghe, C. Detavernier, S. F. Ding, and X. P. Qu, Microelectron. Eng. **88**, 646 (2011).
[14]S. B. S. Heil, P. Kudlacek, E. Langereis, R. Engeln, M. C. M. van de Sanden, and W. M. M. Kessels, Appl. Phys. Lett. **89**, 131505 (2006).
[15]S. B. S. Heil, J. L. van Hemmen, M. C. M. van de Sanden, and W. M. M. Kessels, J. Appl. Phys. **103**, 103302 (2008).
[16]V. R. Rai, V. Vandalon, and S. Agarwal, Langmuir **26**, 13732 (2010).
[17]V. R. Rai and S. Agarwal, J. Phys. Chem. C **113**, 12962 (2009).
[18]S. B. S. Heil, F. Roozeboom, M. C. M. van de Sanden, and W. M. M. Kessels, J. Vac. Sci. Technol. A **26**, 472 (2008).
[19]H. Kim and S. M. Rossnagel, J. Vac. Sci. Technol. A **20**, 802 (2002).
[20]W. J. Maeng, S. J. Park, and H. Kim, J. Vac. Sci. Technol. B **24**, 2276 (2006).
[21]G. B. Rayner and S. M. George, J. Vac. Sci. Technol. A **27**, 716 (2009).
[22]R. Matero, A. Rahtu, and M. Ritala, Chem. Mater. **13**, 4506 (2001).
[23]R. Matero, A. Rahtu, and M. Ritala, Langmuir **21**, 3498 (2005).
[24]L. Henn-Lecordier, W. Lei, M. Anderle, and G. W. Rubloff, J. Vac. Sci. Technol. B **25**, 130 (2007).
[25]*NIST Chemistry WebBook*, http://webbook.nist.gov/chemistry/.
[26]J. H. van Helden, R. A. B. Zijlmans, D. C. Schram, and R. Engeln, Plasma Sources Sci. Technol. **18**, 025020 (2009).
[27]J. H. van Helden, W. Wagemans, G. Yagci, R. A. B. Zijlmans, D. C. Schram, R. Engeln, G. Lombardi, G. D. Stancu, and J. Ropcke, J. Appl. Phys. **101**, 043305 (2007).
[28]P. Violet, I. Nuta, C. Chatillon, and E. Blanquet, Rapid Commun. Mass Spectrom.**24**, 2949 (2010).
[29]B. O. Cho, J. J. Wang, and J. P. Chang, J. Appl. Phys.**92**, 4238 (2002).
[30]B. B. Burton, A. R. Lavoie, and S. M. George, J. Electrochem. Soc. **155**, D508 (2008).
[31]A. J. M. Mackus, S. B. S. Heil, E. Langereis, H. C. M. Knoops, M. C. M. van de Sanden, and W. M. M. Kessels, J. Vac. Sci. Technol. A **28**, 77 (2010).
[32]S. D. Elliott, Langmuir **26**, 9179 (2010).
[33]E. Langereis, J. Keijmel, M. C. M. van de Sanden, and W. M. M. Kessels, Appl. Phys. Lett. **92**, (2008).
[34]D. P. Liu, I. T. Martin, J. Zhou, and E. R. Fisher, Pure Appl. Chem. **78**, 1187 (2006).
[35]F. A. Londry, A. J. Slavin, and P. R. Underhill, Surf. Sci. **140**, 521 (1984).
[36]J. Perrin, M. Shiratani, P. Kae-Nune, H. Videlot, J. Jolly, and J. Guillon, J. Vac. Sci. Technol. A **16**, 278 (1998).
[37]A. von Keudell and W. Jacob, Prog. Surf. Sci. **76**, 21 (2004).
[38]M. F. A. M. van Hest, A. de Graaf, M. C. M. van de Sanden, and D. C. Schram, Plasma Sources Sci. Technol. **9**, 615 (2000).
[39]G. Lombardi, K. Hassouni, G. D. Stancu, L. Mechold, J. Ropcke, and A. Gicquel, J. Appl. Phys. **98**, 053303 (2005).
[40]G. H. Cho and S. W. Rhee, Electrochem. Solid-State Lett. **13**, H426 (2010).
[41]S. H. Kim, M. K. Song, and S. W. Rhee, J. Electrochem. Soc. **157**, H652 (2010).